Two Partial Actinopterygian Neocrania (Occipital Ossifications) from Blue Beach, Nova Scotia

CONRAD D. WILSON,*[,1] CHRIS F. MANSKY,[2] and JASON S. ANDERSON[3]

[1] Department of Earth Sciences, Carleton University, Ottawa, Ontario, K1S 5B6, Canada, conraddwilson@gmail.com;

[2] Blue Beach Fossil Museum, Hantsport, Nova Scotia, B0P 1P0, Canada, bbfossils2023@gmail.com

[3] Faculty of Veterinary Medicine, University of Calgary, Calgary, Alberta, T2R 4N1, Canada, janders@ucalgary.ca;

* Corresponding author

Competing interests: The authors declare there are no competing interests.

Abstract

The earliest Carboniferous Period (Tournaisian stage) is a crucial interval in actinopterygian evolution, but the actinopterygian fossil record for this stage is dominated by flattened specimens referred to inconsistently defined summary taxa. The locality of Blue Beach in Nova Scotia preserves Tournaisian-aged strata of the Horton Bluff Formation and offers a critical window into the actinopterygian fauna. Significantly, actinopterygian specimens from this locality are often preserved in three dimensions, so even partially complete or fragmentary material provides valuable data on actinopterygian morphology and evolutionary dynamics. Here, we describe two partial actinopterygian neocrania from Blue Beach. We review actinopterygian neocranium morphology and the dorsal arterial system to provide a comparative basis identifying these new specimens. We find one neocranium (NSM 017.GF.017.007) is most like early-diverging actinopterygians from the Devonian period; the other (NSM 017.GF.017.004) is most similar to later-diverging Carboniferous actinopterygians. This result underscores the diversity of the actinopterygian fauna preserved in the Horton Bluff Formation and suggests that this fauna was mosaic in composition and non-continuous with derived European actinopterygian faunas. Furthermore, this result contributes to an emerging picture of a gradual transition between Devonian and Carboniferous actinopterygian faunas.

Keywords

Actinopterygii, Carboniferous, braincase, phylogeny, neocranium, Tournaisian

Introduction

A clear shift in the taxonomic make-up of vertebrate faunas occurred at the Devonian-Carboniferous boundary (Sallan and Coates 2010). One prominent hypothesis holds that this faunal turnover was the consequence of a first-order mass extinction (the Hangenberg) affecting

vertebrates (Sallan and Coates 2010). However, a full understanding of the tempo and mode of this transition requires better knowledge of lineage termination and origination. The diversification of early actinopterygians forms a major part of this picture of faunal change, but our knowledge of their interrelationships remains poor (Giles et al. 2017; Coates and Tietjen 2018). A series of recurring Devonian-aged clades have be identified in phylogenetic analysis – including a monophyletic Cheirolepis, Howqualepididae, Moythomasiidae, and Mimiidae (Choo 2012) – but Carboniferous actinopterygians are often recovered in a broad radiation with few stable clades (Giles et al. 2015b; Giles et al. 2017; Wilson et al. 2018; Choo et al. 2019) and their relationship to Devonian actinopterygian groups is unclear (Giles et al. 2022; Henderson et al. 2022a). This instability confounds our understanding of the Devonian-Carboniferous transition in vertebrates as the persistence or loss of actinopterygian lineages cannot be confidently assessed.

New three-dimensionally preserved actinopterygian cranial material of typically Devonian forms in the Carboniferous (e.g., *Avonichthys manskyi*, of Tournaisian age (Wilson et al. 2018)) has demonstrated greater actinopterygian survivorship than expected under a strict mass extinction scenario by adding, as a minimum, a single boundary-crossing lineage. Additionally, typically Carboniferous forms have now been described from the Devonian (e.g., *Palaeoneiros clackorum*, of Famennian age (Giles et al. 2022)). *P. clackorum* was recovered among a clade of derived and otherwise exclusively Carboniferous actinopterygians, ‘pulling’ the divergence ages of many actinopterygian lineages into the Late Devonian period (Giles et al. 2022). Together, these new taxa imply that actinopterygians underwent a cryptic diversification in the Late Devonian period, survived the Hangenberg extinction relatively unscathed, and then

diversified more conspicuously along morphological and functional lines in its aftermath (Giles et al. 2022; Henderson et al. 2022a; Henderson et al. 2022b).

Three-dimensionally preserved actinopterygian cranial material is informative but particularly rare from the early Carboniferous period. A handful of well-described early Carboniferous taxa are known from primarily two-dimensional material (e.g., *Styracopterus fulcratus* and *Fouldenia ischiptera* (Sallan and Coates 2013)), but summary taxa generally dominate the actinopterygian fauna in this interval (Mickle 2017; Henderson et al. 2022b). Early actinopterygian summary taxa (e.g. *Elonichthys*, *Palaeoniscus*, *Rhadinichthys*) lack consistent definitions and the referred material is often poorly preserved and undiagnosable. Despite containing the greater part of described Carboniferous-Permian actinopterygian diversity, these fossils are rarely included in phylogenetic analyses (Mickle 2017).

The locality of Blue Beach, Nova Scotia preserves a diverse earliest Carboniferous (Tournaisian) actinopterygian fauna and has the advantage of preserving three-dimensional material. Previous catalogues of actinopterygian diversity at this locality list either three (*Canobius*, *Elonichthys*, and *Rhadinichthys*) or four (*Acrolepis*, *Elonichthys*, *Rhadinichthys*, and *Palaeoniscus*) genera (Mansky and Lucas 2013). But this restricted fauna belies the abundance of actinopterygian fossil material, including otherwise rare endoskeletal material. The high-energy taphonomic regime at this site (Anderson et al. 2015) has imposed a filter with few exceptions: most braincase specimens include only the anterior part of the neocranium (occipital ossification). The morphology in this region is functionally related to the attachment of the gills and the arterial circulation to the head (the dorsal arterial system) and has provided the basis for previous evolutionary studies and narratives (e.g., Ridewood 1899; Patterson 1975; Schaeffer and Dalquest 1978) prior to the advent of phylogenetic systematics and cladistic methods.

Neocranial morphology related to the dorsal arterial system remains a rich source of character data, allowing for actinopterygian neocrania from Blue Beach to be placed in morphological and evolutionary context using a comparative approach.

Here, we review the morphological disparity of the early actinopterygian dorsal arterial system, define morphotypes, and describe and contextualize two new actinopterygian neocrania from the Tournaisian Horton Group of Blue Beach, Nova Scotia in order to build our understanding of actinopterygian evolution across the Devonian-Carboniferous boundary. We hypothesize that actinopterygians experienced relatively high survivorship across the Hangenberg extinction, resulting in a mosaic early Carboniferous actinopterygian fauna. Thus, we predict that actinopterygian neocrania belonging to Devonian and Carboniferous morphotypes should both be present in the Tournaisian actinopterygian fauna.

Material and methods

Terminology

The neurocranium of almost all early actinopterygians is made up of two ossifications separated by the ventral otic fissure, paired vestibular fontanelles and otico-occipital fissures, and the posterior dorsal fontanelle (Schultze et al. 2022). This produces an L-shaped division such that a ventral extension of the posterior ossification juts forward into the otic region, below the more anterior ossification (Schultze et al. 2022). Schultze et al. (2022) termed the overlapping anterior ossification the paleocranium and the underlapping posterior ossification the neocranium; we follow this terminology here.

Among crown gnathostomes, oxygenated blood is collected from the gills by a series of efferent epibranchial arteries (Liem et al. 2001) (Fig. 1). Elasmobranchs, lungfish, and some actinopterygians additionally receive oxygenated blood from the hyomandibular region via the

efferent hyoidean artery (Poplin 1975) (Fig. 1). These efferent arteries join a dorsal arterial system made up of lateral dorsal aortae which merge posteriorly to form a dorsal aorta (Fig. 1); the dosal aorta carries the oxygenated blood further posteriorly towards the body (Liem et al. 2001). In Palaeozoic non-neopterygian actinopterygians, the lateral dorsal aortae receive blood from both systems, but some efferent epibranchial arteries may join the dorsal aorta directly instead (Poplin 1975). The presence of an aortic canal investing the dorsal aorta is considered diagnostic for Actinopterygii (Gardiner 1984) and the open dorsal arterial system accommodated exclusively by grooves on the neocranium in some Devonian actinopterygians (*Cheirolepis trailli* and *Howqualepis rostridens*) is interpreted as symplesiomorphic with osteichthyans (Giles et al. 2015a). Small occipital arteries may additionally leave the dorsal aorta to irrigate the posterior part of the head (Gardiner 1984). In Palaeozoic non-neopterygian actinopterygians, oxygenated blood was carried anteriorly to the rest of the head by the internal carotids as well as a second set of arteries that diverged anterolaterally from the lateral dorsal aortae, climbed dorsally to reach a notch or foramen on the lateral commissure and passed into the jugular canal, then turned anteriorly towards the orbit (Poplin 1975; Gardiner 1984).

The identity of these arteries has been controversial. Early authors (e.g. Allis (1897), Watson (1928), and Rayner (1951) termed them the external carotid, but later authors (e.g., Poplin (1974, 1975), Patterson (1975), Jarvik (1980), and Gardiner (1984) identified these structures as representing the orbital artery. By contrast, Giles et al. (2015a) observed a laterally curving groove issuing from the grooves for the lateral dorsal aortae and terminating in a foramen on the ventral surface of the anterior neocranium of *Cheirolepis trailli* and interpreted it as housing the efferent hyoidean artery. Giles et al. (2015a) then reinterpreted the grooves and foramina for the “orbital artery” in other Palaeozoic actinopterygians as accommodating the

efferent hyoidean artery. This interpretation has been followed by subsequent authors (e.g., Pradel et al. (2016) and Caron et al. (2023). Giles et al. (2015a) made their argument from position, since the groove and foramen for the "orbital artery" curve posterolaterally and not anteriorly (Giles et al. 2015a; p. 856): "Positionally, this [orbital artery identity] is implausible: it is unlikely that the orbital artery would turn posteriorly, away from the orbit."

However, the orbital artery enters the jugular canal in many actinopterygians before turning towards the orbit, whether through an independent opening or through the canal's open posterior end (Patterson 1975; Jarvik 1980; Gardiner 1984) and may curve posteriorly to do so (e.g. *Polyodon spatula* (Danforth 1912)). On the contrary, it is unclear why a blood vessel collecting from a hemibranch inferred to be present in the hyoid arch (Poplin 1975) should pass into the jugular canal. Indeed, osteological correlates of the efferent hyoidean artery seem to be absent in extant actinopterygians possessing a hemibranch in the hyoid arch (e.g., Lepisosteiformes (Grande 2010; Thiruppathy et al. 2022)). Giles et al. (2015a) reinforced their conclusion by comparison to the putative stem gnathostome *Janusiscus schultzei* (Giles et al. 2015c) and the crown chondrichthyan *Chlamydoselachus anguineus* (Allis 1923). Comparison to broader gnathostome taxa seems apt for *Cheirolepis trailli*, since the condition of the groove transmitting the dorsal aorta in *Cheirolepis* is symplesiomorphic with osteichthyans (Poplin 1975), but less appropriate for more derived actinopterygians with enclosed aortic canals. Therefore, we treat the groove and foramen passing from the lateral dorsal aorta to the jugular canal in many Palaeozoic non-neopterygian actinopterygians as representing the orbital artery but accept that the groove and foramen on the anterior part of the neocranium in *Cheirolepis trailli* could plausibly represent the efferent hyoidean artery.

Material

NSM 017.GF.017.007 is in isolated specimen comprising the ventral otic-region extension and partial occipital region of an actinopterygian neocranium. NSM 017.GF.017.004 comprises the ventral otic-region extension and partial occipital region of an actinopterygian neocranium in loose association with a partially preserved dentary and gill arch elements. Both specimens were collected by CFM (Blue Beach Fossil Museum) in 2017. NSM 017.GF.017.007 and NSM 017.GF.017.004 will be reposited at the Nova Scotia Museum after publication.

Locality

NSM 017.GF.017.007 was found, in situ, in shales of the Blue Beach Member of the Horton Group. NSM 017.GF.017.004 was found as part of a loose slab in the 'gully-slide bonebed', which is made up of slumped sandstones from the Hurd Creek Member of the Horton Bluff Formation. The geological context of the Blue Beach vertebrate fauna has been summarized and reviewed recently by numerous authors, including Mansky and Lucas (2013) and Anderson et al. (2015). Strata of the Horton Bluff Formation at Blue Beach are cyclical and form a coarsening/shallowing-up sequence (Martel and Gibling 1991; Tang et al. 2024). Marine influence appears to have been intermittent and greatest at the base of the exposed section; the palaeoenvironment is interpreted as a lake ranging in depth from nearshore to offshore below wave base (Martel and Gibling 1996; Tang et al. 2024).

Methods

Specimen preparation and photography

CDW prepared NSM 017.GF.017.007 and partially prepared NSM 017.GF.017.004 under an optical microscope using a Paleotools Microjack #1, #2, and #3 airscribe. Allan Lindoe at the University of Alberta completed preparation of NSM 017.GF.017.004 and separated the

184 preserved neocranium and closely associated elements from the larger 'gully-slide bonebed'
185 block. Both specimens were photographed with a Nikon D200 DSLR and a macro lens.
186 *μCT scanning and digital imaging*
187 CDW μCT scanned both specimens in the McCaig Institute for Bone and Joint Health,
188 University of Calgary, Calgary, Alberta with a Skyscan1173 microCT scanner. CDW scanned
189 NSM 017.GF.017.007 at 103 kV and 77 μA, with a 1.00 mm aluminum filter and a voxel size of
190 18.46 μm. CDW scanned NSM 017.GF.017.004 at 130 kV and 61 μA, with a 0.25 mm brass
191 filter and a voxel size of 71.00 μm, imported the image stacks into ImageJ (Schneider et al.
192 2012), cropped them, and downsampled both in the z-axis. NSM 017.GF.017.007 was
193 downsampled by a factor of three and NSM 017.GF.017.004 by a factor of two. Image stacks
194 were segmented in Amira 5.4.0.
195 **Results**
196 **Review of arterial cephalic circulation of non-neopterygian actinopterygians**
197 *Devonian actinopterygians*
198 *Cheirolepis trailli* (Giles et al. 2015a): Closely-spaced grooves for the lateral dorsal aortae are
199 present in the anterior portion of the ventral surface of the neocranium. These reach the straight posterior
200 margin of the ventral otic fissure, recurve laterally, and enter a small foramen interpreted as
201 accommodating the efferent hyoidean artery. The grooves for the lateral dorsal aortae are joined laterally
202 by posteromedially directed grooves starting medial to the vestibular fontanelles and accommodating the
203 efferent epibranchial artery I at a level just anterior to the level of the exit of the vagus nerve. Medial and
204 anterior to this junction, a small peg marks the attachment of the aortic ligament. Posterior to this
205 junction, the grooves for the lateral dorsal aortae and epibranchial arteries I merge to form a single groove
206 for passage of the dorsal aorta – this is open for its entire extent. The dorsal roof of this groove is pierced
207 by a median foramen tentatively identified as serving a branch of the occipital artery.

208 *Howqualepis rostridens* (Long 1988; Giles et al. 2015a): The grooves for the lateral dorsal aortae
209 form a posterior-pointing V in their anterior extent. Posterior to the bifurcation point, the dorsal aorta is
210 carried to the posterior end of the specimen in an open groove. The posterior margin of the ventral otic
211 fissure appears to be straight.
212 *Raynerius splendens* (Giles et al. 2015b): The anterior half of the neocranium is conspicuously
213 marked by grooves for the lateral dorsal aortae. At the level of the straight posterior margin of the ventral
214 otic fissure, the grooves are widely spaced, subparallel and pass medial to the articulation facets for the
215 first infrapharyngobranchial. Posteriorly, the grooves converge as the neocranium expands dorsally along
216 the axis of the otico-occipital fissure; the grooves converge at the level of the vagus nerve. These grooves
217 are joined by shallow, poorly defined, and anterolaterally directed grooves that accommodated efferent
218 arteries. Laterally, the trajectory of the grooves for the lateral dorsal aortae is defined by ridges. These
219 ossifications continue ventrally and medially to form the floor of the aortic canal posterior to the
220 bifurcation point of the lateral dorsal aortae. Although the dorsal aorta is enclosed, its floor is marked at
221 its posterior end by an aortic notch. The lateral walls of the aortic canal, ventral to this notch, appear to be
222 marked by small foramina (pers. obs.) that probably gave passage to the occipital arteries.
223 Only one set of foramina, set laterally on the posterior face of the orbit and communicating
224 posteriorly with the jugular canal, are labelled for the orbital artery. However, a second set of foramina
225 pierces the outer wall of the jugular canal (pers. obs.) – it seems likely that these gave the orbital artery
226 passage into the jugular canal, from which it supplied blood to the orbit. This is consistent with previous
227 interpretations of similar foramina in other Palaeozoic actinopterygians (e.g. *Kansasiella eatoni* (Poplin
228 1974)).
229 *Mimipiscis toombsi* (Gardiner 1984): Posterior to the level of the straight posterior margin of the
230 ventral otic fissure, the grooves for the lateral dorsal aortae curve around the articulation facet for the first
231 infrapharyngobranchial to form a posterior-pointing V in the anterior half of the ventral surface of the
232 neocranium. In some specimens (Gardiner (1984), Figs. 14 and 15), a poorly defined, shallow, and
233 anterolaterally directed groove appears to branch from the lateral dorsal aortae, similar to the condition in

Raynerius splendens. The bifurcation point of the lateral dorsal aortae is open in all specimens except for one idiosyncratic (Gardiner 1984; Choo et al. 2019) specimen in which the enclosed bifurcation point and subparallel grooves for the lateral dorsal aortae are reminiscent of *Pickeringius acanthophorus* and *Avonichthys manskyi*. The posterior point of the raised triangular area medial to the grooves for the lateral dorsal aortae alternatively bears a protuberance or ridge for the attachment of the aortic ligament. The dorsal aorta is enclosed posterior to the bifurcation point of the lateral dorsal aortae – it is variably pierced, laterally, by one or two foramina that accommodated the occipital artery.

The orbital artery was carried from its division from the lateral dorsal aortae at the ventral otic fissure in a groove that curves laterally and posteriorly around the articulation facet for the first infrapharyngobranchial before beginning a dorsal climb. This groove terminates in a posterior notch in the outer wall of the jugular canal which would accommodate the entrance of the orbital artery.

Moythomasia durgaringa (Gardiner 1984; Long and Trinajstic 2010)**:** The neocranium of *Moythomasia durgaringa* is incompletely described (Giles et al. 2015b). However, Long and Trinajstic (2010), fig. 5b) published a photograph of the ventral surface of the neocranium in this taxon. It appears that the lateral dorsal aortae were carried in widely-spaced, subparallel grooves in the anterior half of the neocranium, before forming a posterior-pointing V. No ventral foramina communicating with the aortic canal appear to be present. The bifurcation point of the lateral dorsal aortae is open and the floor of the aortic canal is marked posteriorly by an aortic notch (Choo et al. 2019).

No groove for the orbital artery is apparent in the photograph (Long and Trinajstic, 2010, fig. 5b), but a foramen in the outer wall of the jugular canal, lateral and dorsal to the articulation facet for the first infrapharyngobranchial, is apparent. This is congruent with the lateral reconstruction of Gardiner (Gardiner 1984), in which a dorsally-directed groove reaches the orbital artery foramen from the ventral otic fissure.

Palaeoneiros clackorum (Giles et al. 2022): The neocranium of the only known specimen of this taxon is fragmentary. It is nevertheless significant because it is the only known Devonian actinopterygian

with an independent ventral foramina communicating with the aortic canal that would have accommodated efferent epibranchial arteries.

Pickeringius acanthophorus (Choo et al. 2019): The lateral dorsal aortae were carried in widely-spaced and subparallel grooves posteriorly from the ventral otic fissure in this taxon (Choo et al. 2019, fig. 3d-f). Posteriorly, these grooves for the lateral dorsal aortae pass separately into canals – the bifurcation point of the lateral dorsal aortae is enclosed. The dorsal aorta is also enclosed in an aortic canal and there are no ventral foramina communicating with the aortic canal. There is no aortic notch.

Although the orbital artery is undescribed, there appears to be a foramen in the outer wall of the jugular canal in a similar position to the orbital artery foramen described in other actinopterygian taxa.

Carboniferous actinopterygians

Avonichthys manskyi (Wilson et al. 2018)*:* Posterior to the straight posterior margin of the ventral otic fissure, the ventral surface of the neocranium is marked by paired, subparallel grooves for the lateral dorsal aortae. These diverge anteriorly and curve around articulation facets for the first infrapharyngobranchial. The bifurcation point of the lateral dorsal aortae is enclosed. The specimen ends posteriorly, and no foramina piercing the aortic canal are preserved. However, the ventral surface of the aortic canal is marked by anteriorly divergent grooves (pers. obs.) similar to those interpreted as marking the passage of efferent epibranchial arteries III and IV in *Lawrenciella schaefferi* (Pradel et al. 2016). Incomplete preservation precludes description of the orbital artery.

Coccocephalus wildi (Poplin and Véran 1996): Grooves for the lateral dorsal aortae form a posterior-pointing V in the anterior half of the ventral surface of the neocranium. These are curved laterally, just posterior to the posteriorly convex posterior margin of the ventral otic fissure, around the articulation facets for the first infrapharyngobranchial. Posteriorly and laterally, these grooves are joined by a shallow pair of anterolaterally directed grooves. Immediately medial to this junction, the triangular area is marked by a pair of notches – Poplin and Véran (1996) made no identification of these beyond a suggestion that they might represent orbitonasal arteries. Posterior to this, the bifurcation point of the lateral dorsal aortae is open, whereas the rest of the dorsal aorta is enclosed. The aortic canal is pierced by

a ventral and median foramen interpreted by Poplin and Véran (1996) as accommodating efferent epibranchial arteries II-IV and, posterior, lateral, and dorsal to this, by a set of foramina accommodating the exit of the occipital arteries.

Grooves for the orbital artery curve laterally around the articulation facets for the first infrapharyngobranchial, then climb dorsally and posteriorly towards a notch on the posterior edge of the outer wall of the jugular canal.

Cosmoptychius striatus (Watson 1928; Schaeffer 1971)**:** The neocranium of *Cosmoptychius striatus* was originally described and illustrated by Watson (1928, fig. 3) from an incompletely ossified (presumably immature (Schaeffer 1971)) partial neurocranium. Subsequent redescription and new illustrations by Schaeffer (1971, fig. 8) yielded some differences in the position of foramina for efferent epibranchial arteries. We follow the latter source here.

Short grooves for the lateral dorsal aortae are restricted to the anterior fifth of the ventral surface of the neocranium. These curve laterally around the articular facet for the first infrapharyngobranchial. There is a small foramen posterior to this facet and lateral to the grooves for the lateral dorsal aortae – this gave passage to efferent epibranchial artery I. Posterior to this, the grooves for the lateral dorsal aortae become canals, so the bifurcation point of the lateral dorsal aortae is enclosed. There are no other ventral foramina piercing the aortic canal, although there is an aortic notch (Schaeffer, 1971, fig. 8). No foramina for the occipital artery are apparent.

Kentuckia deani (Rayner 1951)**:** Grooves for the lateral dorsal aortae form a posterior-pointing V in the anterior third of the ventral surface of the neocranium. Immediately posterior to the straight posterior margin of the ventral otic fissure, the grooves for the lateral dorsal aortae are joined by a pair of anterolaterally directed grooves for efferent epibranchial artery I. The bifurcation point of the lateral dorsal aortae is not enclosed, but the dorsal aorta is enclosed posterior to this point. The aortic canal is pierced, in the posterior half of the neocranium, by a single median foramen giving passage to efferent epibranchial arteries. The aortic canal appears to deepen (Rayner, 1951, fig. 9) posterior to the entrance of

the epibranchial arteries. Posterior and dorsal to this, the lateral walls of the cranial aorta bear two sets of paired foramina – these accommodated occipital arteries.

The orbital artery is not described. However, a foramen for the orbital artery present on the outer wall of the jugular canal, dorsal, lateral, and slightly posterior to the ventral otic fissure.

Kansasiella eatoni (Poplin 1974)**:** The anterior part of the ventral surface of the neocranium bears short and anteriorly restricted grooves for the lateral dorsal aortae. These travel anterolaterally and appear to intersect the posteriorly convex posterior margin of the ventral otic fissure obliquely. The enclosed bifurcation point of the lateral dorsal aortae is immediately posterior to the ventral otic fissure (Choo et al. 2019). Posterior to the level of the vestibular fontanelles, the aortic canal is pierced by paired canals that accommodated efferent epibranchial arteries. These run ventrolaterally and are visible in both lateral and ventral view. The cranial aorta increases in cross-sectional area posterior to the entrance of the efferent epibranchial arteries. In the posterior third of the neocranium, the lateral walls of aortic canal are marked dorsally by paired foramina that accommodated the occipital artery (Gardiner 1984).

The orbital artery curves laterally across the ventral otic fissure then climbs dorsally to a foramen on the outer wall of the jugular canal.

Lawrenciella schaefferi (Poplin 1984; Hamel and Poplin 2008; Pradel et al. 2016)**:** Grooves for the lateral dorsal aortae are short, laterally directed, and anteriorly restricted. Posteriorly, these grooves transition into canals anterior to the level of the vestibular fontanelles and then converge, such that the enclosed bifurcation point of the lateral dorsal aortae is immediately posterior to the posteriorly convex posterior margin of the ventral otic fissure (Choo et al. 2019). The aortic canal is pierced, just posterior to the level of the vestibular fontanelles, by a median, ventral foramen that accommodated epibranchial arteries. In at least one specimen (Pradel et al. 2016, fig. 5), the ventral surface of the aortic canal is marked by paired grooves that diverge anteriorly – these likely accommodated a common root of efferent epibranchial arteries III and IV (Pradel et al. 2016). The dorsal part of the aortic canal is also pierced, laterally, by foramina for the occipital artery.

Grooves for the orbital artery diverge from the lateral dorsal aortae and follow the posterior margin of the ventral otic fissure, curve around articulation facets for the first infrapharyngobranchial, then travel dorsally and posteriorly to reach a set of foramina dorsal and lateral to the exit of the lateral dorsal aortae.

Phoebeannaia mossae (Caron et al. 2023):

The dorsal arterial system of this taxon appears very similar to that of *Kansasiella eatoni* except in the configuration of the foramina piercing the aortic canal for the passage of the efferent epibranchial arteries. The anterior part of the neocranium is marked by wide, divergent grooves that accommodated the lateral dorsal aortae. The anterior end of the aortic canal is defined by the divergence of the grooves for the lateral dorsal aortae. Unlike *Kansasiella eatoni*, the aortic canal is pierced by a single median foramen that accommodated efferent epibranchial arteries posterior to the widening of the of oticooccipital fissure that accommodated cranial nerve X. Articular surfaces for the first infrapharyngobranchial are present anterior and lateral to the grooves for the lateral dorsal aortae. An additional set of paired grooves curve around the articular facets and rise posteriorly towards foramina on the lateral commissure communicating with the jugular canal; these would have accommodated the orbital arteries.

Woodichthys bearsdeni (Coates 1998)**:** Short, anteriorly restricted grooves for the lateral dorsal aortae are present on the ventral surface of the neocranium. The bifurcation point of the lateral dorsal aortae is enclosed; posterior to this, the long aortic canal is pierced medially and ventrally by a single foramen for efferent epibranchial arteries. No occipital artery is indicated by Coates (1998).

Permian actinopterygians

Luederia kempi (Schaeffer and Dalquest 1978)**:** The ventral surface of the anterior part of the neocranium is marked by short, subparallel, and anteriorly restricted grooves for the lateral dorsal aortae running medial to the articulation facet of the first infrapharyngobranchial and lateral to the posteriorly-extended parasphenoid. The ventral otic fissure is not marked by perichondral bone but is instead filled with cancellous bone. Grooves accommodating the lateral dorsal aortae and orbital artery are present in the anterior 1/3rd of the neocranium. These grooves transition into canals which are pierced, posteriorly,

by a pair of more medially set openings for efferent epibranchial arteries. The position of the enclosed bifurcation point of the lateral dorsal aortae is unclear. The aortic canal is pierced again, posterior to the level of the vestibular fontanelles, by a median, ventral opening that accommodated other efferent epibranchial arteries. Dorsal to this, the lateral wall of the aortic canal is marked by a foramen for the occipital artery.

Grooves for the orbital artery diverge laterally from the grooves for the lateral dorsal aortae and curve around the anterior edge of the articulation facet of the first infrapharyngobranchial, climb dorsally, and reach a slot on the outer wall of jugular canal.

Triassic actinopterygians

Pteronisculus stensioi (Nielsen 1942): The ventral surface of the anterior part of the neocranium is marked by subparallel grooves for the lateral dorsal aortae. Just posterior to the gently posteriorly convex posterior margin of the ventral otic fissure, these are joined, laterally, by anterolaterally directed grooves accommodating efferent epibranchial artery I. These grooves curve sharply towards the anterior and appear to leave the ventral surface of the neocranium obliquely. The grooves for the lateral dorsal aortae converge slightly, then transition into canals. The enclosed bifurcation point of the lateral dorsal aortae is slightly posterior to their entrance into canals. The dorsal aorta is pierced, in the posterior third of the neocranium by a median, ventral foramen accommodating efferent epibranchial arteries. Lateral to this, the dorsal part of the aortic canal is pierced by a foramen for the occipital artery. The 'triangular area' between the lateral dorsal aortae is marked by a longitudinal trough interpreted by Bjerring (1971) as an insertion for subcephalic musculature.

The groove for the orbital artery diverges laterally and anteriorly from the lateral dorsal aortae, crosses the ventral otic fissure, curves posteriorly around the articulation facet of the first infrapharyngobranchial, and climbs dorsally to reach a foramen in the outer wall of the jugular canal.

Australosomus kochi (Nielsen 1949): Curved grooves for the lateral dorsal aortae mark the ventral surface of the anterior neocranium. Although these diverge anteriorly, towards the straight posterior margin of the ventral otic fissure, they remain tightly spaced and define a narrow, raised

triangular area that bears a median process for the attachment of the aortic ligament (Nielsen 1949; Patterson 1975). The bifurcation point of the lateral dorsal aortae is open and a long, anteriorly-open slot in the floor of the neocranium exposes the aortic canal. Lateral to this, the dorsal part of the aortic canal is marked by a foramen for the occipital artery. The slot is closed at its posterior end and the dorsal aorta is enclosed up to its exit from the neocranium.

The orbital artery crosses the ventral otic fissure, curves posteriorly and climbs dorsally and laterally to a foramen on the outer wall of the jugular canal.

Description of NSM 017.GF.017.007

NSM 017.GF.017.007 (Figs. 2-4) comprises the anteroventral portion of an actinopterygian neocranium, including the ventral otic-region extension and part of the occipital region. Although the anterior part of the specimen appears complete up to the presumed level of the ventral otic fissure, it is broken medial to the vestibular fontanelles. The posterior end of the specimen occurs slightly posterior to the exit of the occipital artery at the level of the notochordal canal (Figs. 2 and 3).

The anterior portion of the specimen is conspicuously marked by paired, V-shaped, shallow grooves for passage of the lateral dorsal aortae (lda, Figs. 2-4). These curve laterally as they approach the presumed level of the straight posterior margin of the ventral otic fissure – this may indicate the divergence of the orbital artery (oa, Fig. 2) from the internal carotid artery (i.car, Fig. 2). On the left side of the specimen, the left lateral dorsal aorta is flanked by a raised, rounded and rough-textured area that likely represents the articulation facet for the first infrapharyngobranchial (?aip1, Fig. 2). The equivalent area on the right side of the specimen is not raised, although its texture is also rough. From the ventral otic fissure, the grooves turn posteriorly and travel towards a median bifurcation point. The overall trajectory of the grooves for the lateral dorsal aortae is reminiscent of *Mimipiscis toombsi*, *Howqualepis rostridens*,

411 *Coccocephalus wildi*, and *Kentuckia deani*. The grooves for the lateral dorsal aortae are joined
412 laterally, about two-thirds of the way along their posterior trajectory, by a pair of
413 posteroventrally directed grooves (eff, Figs. 2 and 4) that accommodated efferent arteries.
414 Similar laterally-diverging grooves are also present in *Cheirolepis trailli*, *Mimipiscis toombsi*,
415 *Raynerius splendens*, *Coccocephalus wildi*, and *Kentuckia deani*, although the grooves in
416 *Kentuckia deani* are more anterior and better defined than in the other taxa. Immediately anterior
417 to these efferent grooves, the medially inclined medial walls of the grooves for the lateral dorsal
418 aortae are marked by a pair of dorsoposteriorly directed notches (?ona, Fig. 2). A similar
419 structure is observed in *Coccocephalus wildi* (Poplin and Véran 1996) and *Ligulalepis* (Basden
420 and Young 2001). In the latter, these were suggested to give passage to orbitonasal arteries
421 (Basden and Young 2001). The grooves for the lateral dorsal aortae continue their V-shaped
422 trajectory and converge just posterior to the position of the orbitonasal arteries. The raised
423 triangular area between the lateral dorsal aortae is marked anteriorly by a gradual lip along its
424 anterior margin. The posterior apex of the triangle bears a raised, round boss (a.peg, Figs. 2 and
425 4); Gardiner (1984) interpreted a similar structure in some specimens of *Moythomasia*
426 *durgaringa* as an attachment point for an aortic ligament.
427 The point where the grooves for the lateral dorsal aortae converge is open, as in
428 *Cheirolepis trailli*, *Mimipiscis toombsi, Moythomasia durgaringa*, *Raynerius splendens*,
429 *Kentuckia deani*, *Coccocephalus wildi*, and *Australosomus kochi*. A thin, ventral bony cover of
430 the aortic canal (cao, Figs. 2 and 4) just posterior to this was inadvertently removed by
431 overpreparation after μCT scans were taken, but μCT data demonstrate that the dorsal aorta (da,
432 Fig. 3) was carried exclusively in a canal posterior to the bifurcation point in the original
433 specimen. The aortic canal (cao, Figs. 2 and 4) deepens posteriorly. Immediately anterior to its

deepest point, the dorsal margin of the aortic canal is pierced by a lateral pair of foramina (foca, Fig. 2); these accommodated the exit of the occipital arteries (oca, Fig. 3). The foramina for the occipital arteries occur in the posterior third of the specimen. As the occipital arteries exit relatively posteriorly in diverse non-neopterygian actinopterygians (e.g. *Mimipiscis toombsi* (Gardiner 1984, fig. 13); *Moythomasia durgaringa* (Gardiner 1984, fig. 7); *Kentuckia deani* (Rayner 1951), Fig. 9; and *Pteronisculus stensioi* (Nielsen 1942, fig. 11), the position of the occipital artery foramina in this specimen suggests little of the posterior extent of the neocranium was not preserved. There is no evidence for additional ventral or lateral foramina piercing the aortic canal. Whereas specimen incompleteness has exposed the aortic canal on the right side of the specimen, the nearly complete left side indicates that the aortic canal did not open ventrally (Figs. 2-4). Furthermore, we are not aware of any non-neopterygian actinopterygians with foramina for efferent epibranchial arteries completely posterior to the occipital arteries. This seems to indicate that additional foramina for efferent epibranchial arteries were not present in this specimen and thus that all efferent epibranchial arteries reaching the neocranium drained into the lateral dorsal aortae. Efferent epibranchial artery penetration of the aortic canal is also absent in *Mimipiscis toombsi*, *Moythomasia durgaringa*, *Raynerius splendens*, *Pickeringius acanthophorus*, and *Cosmoptychius striatus* (although the lateral dorsal aortae are pierced laterally by foramina for efferent epibranchial artery I in this taxon).

Part of the notochordal canal is preserved in the dorsal part of the specimen, but its roof is missing due to incomplete preservation (nc, Fig. 3). The notochord appears to be deepest posteriorly but becomes shallow anterior to the level of the occipital arteries.

Description of NSM 017.GF.017.004

NSM 017.GF.017.004 (Figs. 5-7) comprises the anteroventral portion of an actinopterygian neocranium in loose association with a small dentary (den1, Fig. 5) and a gill arch element (?eb, Figs. 5 and 6). This smaller specimen was removed from a larger gully-slide bonebed slab which preserves actinopterygian scales and additional mandibular material (den2 and den3, Fig 5). The anterior part of the neocranium appears complete to the presumed level of the ventral otic fissure; however, the neocranium is broken lateral to the lateral dorsal aortae. The neocranium is crushed and incomplete dorsally and posteriorly: the incomplete dorsal portion of the right lateral wall of the neocranium extends posterior to the end of preservation of the aortic canal (cao, Fig. 6). There are no foramina for the occipital artery apparent in the neocranium, nor any articulation facets for the first infrapharyngobranchial.

The anterior part of the neocranium bears paired grooves for the lateral dorsal aortae (lda, Figs. 6 and 7). These reach the straight posterior margin of the ventral otic fissure. The grooves appear shallow and subparallel in their anterior extent, although the absence of their lateral walls indicates specimen incompleteness. The configuration of these grooves is reminiscent of *Pickeringius acanthophorus*, *Avonichthys manskyi*, *Cosmoptychius striatus*, *Pteronisculus stensioi*, and a specimen of *Elonichthys aitkeni* illustrated by Watson (1925, fig. 23). Posteriorly, the grooves for the lateral dorsal aortae undertake a serpentine curve – narrowing the space between them – before deepening and transitioning into canals (lda, Figs. 6 and 7).

The sub-rectangular area between the grooves for the lateral dorsal aortae is marked by a shallow, median trough (md, Fig. 6). This likely represents a muscular attachment area, but the identity of this muscle has been controversial (Bjerring 1971; Patterson 1975). The slope defining the median trough is steepest posteriorly, becoming more gradual laterally and anteriorly. There is no evidence of an attachment point for an aortic ligament in this area.

The grooves for the lateral dorsal aortae pass into canals in the anterior third of the specimen. These canals are pierced immediately posterior to the end of the grooves, by a pair of laterally curving canals leading to a small, lateral, and ventrally situated pair of foramina for the passage of efferent epibranchial artery I (epi.1, Figs. 6 and 7). This is strongly reminiscent of the lateral exit of canals for efferent epibranchial artery I in *Cosmoptychius striatus* (Schaeffer 1971) and, to a lesser extent, *Kansasiella eatoni* (Poplin 1974). The paired canals for the lateral dorsal aortae continue a V-shaped trajectory posteriorly, forming an enclosed bifurcation point in the posterior half of the specimen. The dorsal aorta (da, Figs. 6 and 7) is carried exclusively in a canal posterior to the bifurcation point. This continuation of separate channels for the lateral dorsal aortae posterior to their entrance into canals is similar to *Pteronisculus stensioi*. The exterior surface of the neocranium ventral to this bifurcation point is eroded and the aortic canal is exposed on the left lateral side of the mid-sagittal plane (Fig. 6). Anterior to this damage, the specimen seems to bear a symmetrical pair of crescentic grooves, but only one communicates with the aortic canal, via the eroded portion of the specimen (Fig. 6). It therefore seems unlikely that these represent foramina for additional (II-IV) efferent epibranchial arteries. Similarly, there are no foramina for the occipital artery preserved in this specimen. However, the posterior incompleteness means that the presence of these, or of additional foramina for efferent epibranchial arteries, cannot be ruled out.

An element that is probably an epibranchial (?eb, Fig. 6) contacts the right side of the neocranium. This element is poorly preserved and does not resolve well in μCT. A fragmentary actinopterygian dentary is also included in the small μCT-scanned block in loose association with the neocranium (den1, Fig 5). The dentary is long and linear and its lateral surface is ornamented in vermiform ridges of hypermineralized tissue and marked ventrally by the

impression of the mandibular canal. Additional mechanical preparation of the specimen revealed the presence of two rows of teeth represented by a row of small marginal teeth and a solitary large tooth towards the distal end of the jaw. Because of the high relative abundance of mandibular material (Fig. 5; the parent slab for NSM 017.GF.017.004 alone preserves at least three mandibles) in the gully-slide bonebed and the loose association of the dentary with the neocranium, it is unclear if these elements belong to the same animal. Thus, we focus this study on the neocranial material alone. The abundant mandibular material preserved at Blue Beach will be described in upcoming papers.

Discussion

The neocranial morphotype of Devonian actinopterygians

The neocranium of Devonian actinopterygians (excepting *Palaeoneiros clackorum* (Giles et al. 2022)) varies in the presence or absence of a canal-invested dorsal aorta and the enclosure of the bifurcation point of the lateral dorsal aortae (Fig. 8). Devonian actinopterygians generally have widely-spaced, V-shaped grooves for the lateral dorsal aortae, but these are also present in Carboniferous taxa like *Coccocephalus wildi* and *Kentuckia deani* (Choo et al. 2019). Critically, in Devonian taxa, the absence of foramina for the efferent epibranchial arteries piercing the aortic canal (present in *Kentuckia deani*, *Coccocephalus wildi*, and other Carboniferous-Permian actinopterygians) in combination with poorly-defined, relatively wide channels diverging from the lateral dorsal aortae (present in the Devonian taxa *Raynerius splendens*, *Moythomasia durgaringa* and *Mimipiscis toombsi*) suggests that all efferent epibranchial arteries entering the neocranium were received by the lateral dorsal aortae (Poplin 1975) (Fig. 8). This characterizes the neocranial morphotype of Devonian actinopterygians.

The neocranial morphotype of post-Devonian actinopterygians

525 Carboniferous-Permian actinopterygians display wide variation in their cephalic arterial
526 circulation, especially in the bifurcation point of the enclosed dorsal aorta and the shape of the
527 grooves for the lateral dorsal aortae (Fig. 8). However, these taxa all bear foramina in the canal
528 for the dorsal aorta. These allowed efferent epibranchial arteries to pierce the neocranium and
529 join the dorsal aorta directly (Poplin 1975). This feature primarily characterizes the neocranial
530 morphotype of Carboniferous-Permian actinopterygians.

531 **Identity of NSM 017.GF.017.007**

532 The general arrangement of the dorsal aortic system (with posterior pointing V-shaped
533 grooves for the lateral dorsal aortae, an open bifurcation point, and the dorsal aorta carried in a
534 canal) in NSM 017.GF.017.007 is reminiscent of many Devonian and Carboniferous
535 actinopterygians, especially *Mimipiscis toombsi*, *Kentuckia deani*, and *Coccocephalus wildi* (Fig.
536 8).

537 The small grooves on the medial wall of the lateral dorsal aortae are similar to
538 unidentified grooves in *Coccocephalus wildi* which Poplin and Véran (1996) identified as
539 probably accommodating the orbitonasal arteries. However, there are other points of difference
540 with *Coccocephalus wildi*: the ventral otic fissure is posteriorly convex in *C. wildi* and straight in
541 this specimen; and the peg for attachment of the aortic ligament present in this taxon is not
542 indicated in *C. wildi*. The condition of the occipital arteries is a point of difference with
543 *Kentuckia deani* – each lateral set is paired in *K. deani* and single in this specimen – although
544 this difference falls within species-level variation known for *Mimipiscis toombsi* (Gardiner
545 1984).

546 However, the configuration of the efferent epibranchial arteries in this specimen is unlike
547 *Coccocephalus wildi* and *Kentuckia deani* but more similar to Devonian actinopterygians.

Whereas the specimen is posteriorly incomplete, the observation that the aortic canal is closed posterior to the exit of the occipital arteries strongly suggests that no efferent epibranchial foramina were present. This, together with the wide channels diverging from the lateral dorsal aortae, indicates that all efferent epibranchial arteries drained into the lateral dorsal aortae.

Thus, the configuration of the efferent epibranchial arteries means that NSM 017.GF.017.007 best matches the neocranial morphotype of Devonian actinopterygians. Among these, the configuration of grooves for the lateral dorsal aortae is most similar to *Mimipiscis toombsi*.

Identity of NSM 017.GF.017.004

The general configuration of the dorsal aortic system (with subparallel grooves for the lateral dorsal in the anterior neocranium that pass into canals posteriorly, an enclosed bifurcation point, and the dorsal aorta carried in a canal) in NSM 017.GF.017.004 is reminiscent of many non-neopterygian actinopterygians, including *Avonichthys manskyi*, *Pickeringius acanthophorus*, *Cosmoptychius striatus*, and *Pteronisculus stensioi* (Fig. 8).

The presence of foramina piercing the dorsal aorta and presumably accommodating efferent epibranchial arteries establishes this specimen in the Carboniferous-Permian actinopterygian neocranial morphotype. In NSM 017.GF.017.004 these canals are laterally directed, similar to those present in *Cosmoptychius striatus*. However, unlike *Cosmoptychius striatus*, there are no articulation facets for the first infrapharyngobranchial preserved anterior and medial to the foramina for efferent epibranchial arteries I. The absence of these structures from the specimen may be taphonomic, as the specimen is laterally incomplete – but these articulation facets are also absent in derived non-neopterygian actinopterygians in which the first infrapharyngobranchial articulates with the parasphenoid (e.g. *Pteronisculus stensioi* (Nielsen

1942)). The presence of a long, deep, median depression (likely acting as a muscle attachment area) in the anterior part of the neocranium is a further point of difference between this specimen and known Devonian taxa; this feature is otherwise known in *Pteronisculus stensioi*. Bjerring (1971) interpreted this feature in *P. stensioi* as an insertion point for subcephalic muscles originating on the parasphenoid, but Patterson (1975) argued that this and similar triangular areas between grooves for the lateral dorsal aortae in other taxa could just as easily be an insertion for anterior musculature continuous with the trunk musculature. Because a triangular area (albeit raised and without a median depression) is present in *Moythomasia toombsi*, *Mimipiscis toombsi*, and *Kentuckia deani*, Patterson (1975) inferred that such an attachment was primitive for actinopterygians. The tightly spaced lateral dorsal aortae of *Cheirolepis trailli* (Giles et al. 2015a, fig. 5) may not have allowed such an attachment (as Patterson (1975) argued for *Australosomus kochi*), although a triangular area is apparently present between the V-shaped lateral dorsal aortae of *Howqualepis rostridens* (Giles et al. 2015a, fig. 12). In any case, it seems probable that the position and arrangement of the muscular insertion is tightly correlated with the configuration of the cephalic arterial circulation (because the presence or absence and position of grooves for the lateral dorsal aortae defines the triangular area) and the parasphenoid (because posterior parasphenoid overlap of the ventral otic fissure and anterior neocranium, as in many relatively derived Permian-Triassic actinopterygians, alters muscle attachment patterns (Patterson 1975)).

Unfortunately, the poorly resolved structure of the Carboniferous-Permian actinopterygian radiation makes precise identification of NSM 017.GF.017.004 with a specific actinopterygian group difficult. However, the presence of foramina piercing the enclosed dorsal aorta and accommodating efferent epibranchial arteries in this specimen establish it within the

neocranial morphotype of post-Devonian actinopterygians. The specimen is most similar to the neocrania of *Cosmoptychius striatus* and *Pteronisculus stensioi* that have previously been recovered as derived members of a Carboniferous-Permian actinopterygian radiation (e.g. Giles 2015b, fig. 5; Choo et al. 2019, fig. 14; Friedman, 2015, fig. 3).

Environmental Bias and Homoplasy

Other than *Cheirolepis trailli* and *Howqualepis rostridens*, the Devonian actinopterygian braincase record appears to be environmentally biased towards reef environments (*Mimipiscis toombsi*, *Moythomasia durgaringa*, *Gogosardina coatesi*, and *Pickeringius acanthophorus* were preserved in an inter-reef basinal Lagerstätte (Long and Trinajstic 2010); and *Raynerius splendens*, was preserved in a shallow marine and reef-associated environment (Mistiaen et al. 2012; Giles et al. 2015b)). This contrasts with environmental data for Carboniferous braincases. Actinopterygian neocrania from marine (*Coccocephalus wildi* (Poplin and Véran 1996)), nearshore marine (*Kansasiella eatoni* (Poplin 1974), *Kentuckia deani* (Eastman 1907), *Lawrenciella schaefferi* (Hamel and Poplin 2008), and *Woodichthys bearsdeni* (Sallan and Coates 2010)), and nonmarine (*Cosmoptychius striatus* (Sallan and Coates 2010)) settings are all known, whereas specifically reefal environments are not represented in the Carboniferous. Thus, differences between Devonian and Carboniferous actinopterygian braincases could reflect ecology. However, no reefal influence is apparent at Blue Beach, so the similarities between the neocrania of Devonian reefal actinopterygians and NSM 017.GF.017.007 are not driven by similarity in environment. Similarities between NSM 017.GF.017.004 and derived members of the Carboniferous-Permian actinopterygian radiation also seem unlikely to be driven by convergent adaptation to similar environments because NSM 017.GF.017.004 is similar to a actinopterygians from disparate environmental settings.

Even if morphological convergence between these new specimens and other Palaeozoic actinopterygians due to shared ecology or environment seems unlikely, broader concerns about homoplasy between the specimens presented in this study and the rest of the actinopterygian braincase record remain. This is especially the case with NSM 017.GF.017.007, as the specimen is identified with early-diverging Devonian actinopterygians based on the apparently plesiomorphic condition of its dorsal aortic system (with all efferent epibranchial arteries reaching the neocranium draining into the open lateral dorsal aortae). By contrast, the placement of NSM 017.GF.017.004 is supported by clear apomorphies. The embayment of the triangular area of the anterior neocranium and the anterolateral, canalized entrance of efferent epibranchial artery I into the neocranium appear to be acquired within the Carboniferous-Permian actinopterygian radiation.

Horton Bluff Formation actinopterygian diversity

The specimens described in this study underscore the diversity of actinopterygians preserved in the Horton Bluff Formation. These specimens, in combination with known platysomid material (Wilson et al. 2021) and *Avonichthys manskyi* (Wilson et al. 2018), suggest that at least four actinopterygian lineages were present in the Horton Bluff Formation. This diversity is not additive to the previously catalogued actinopterygian diversity (e.g. Gardiner, 1966; Sallan and Coates, 2010; Mansky and Lucas, 2013): the relationship of these new specimens to that fauna is unclear as the preserved anatomy does not overlap. The diversity represented by neocrania at Blue Beach could overlap with any of the summary taxa known from the Horton Bluff Formation.

These summary genera (i.e. *Acrolepis*, *Elonichthys*, *Palaeoniscus, Rhadinichthys* (Sallan and Coates 2010) and *Canobius* (Mansky and Lucas 2013)) generally represent taxa erected for

640 the European Carboniferous-Permian actinopterygian fauna and the contemporaneous Albert
641 Mines locality (Gardiner 1966). This naming convention falsely makes the Blue Beach fauna
642 appear derived relative to the actinopterygian fauna preserved at Devonian sites. Instead, our
643 interpretation of actinopterygian neocrania preserved at Blue Beach suggests that a mix of
644 Devonian-like and Carboniferous-like actinopterygians were present in the fauna. By preserving
645 representatives of both faunas, the Blue Beach fauna appears distinct from the derived
646 Carboniferous-Permian actinopterygian fauna preserved elsewhere. This mirrors recently
647 published phylogenetic results with topologies suggesting high actinopterygian survivorship
648 across the Devonian-Carboniferous boundary (Giles et al. 2022) and results suggesting relatively
649 high survivorship in lungfishes (Challands et al. 2019) and tetrapods (Anderson et al. 2015;
650 Clack et al. 2016; Smithson et al. 2024).

651 **Characters of the actinopterygian dorsal arterial system**

652 Recent research emphasis on early actinopterygian cranial material and braincase
653 character evolution has brought a renewed focus on the actinopterygian dorsal arterial system
654 Giles et al. (2015b), Giles et al. (2017), Giles et al. (2022), and Caron et al. (2023) each listed
655 characters related to the actinopterygian dorsal arterial system in their analyses. We propose the
656 addition of the following three characters to the four retained from Caron et al. (2023), Giles et
657 al. (2015b), and Giles et al. (2017).

658 Characters proposed in this study:

659 1. **Entrance of paired efferent epibranchial arteries in anterior half of neocranium:**
660 **absent/present.** Lateral entrances for paired efferent arteries in the anterior part of the
661 neocranium are widespread among actinopterygians, but some (e.g. *Boreosomus* (Nielsen
662 1942)) lack these entrances. This character seems to have implications for how

oxygenated blood is collected by the main arterial system. Previous authors (e.g., Poplin (1975), Giles et al. (2015b), and Giles et al. (2017)) have assigned these entrances to different efferent arteries. Instead, we formulated our definition to avoid inference of the exact efferent artery represented by the entrance. Together with Character 3 (outlined below), this is intended to replace characters 113 and 114 in Giles et al. (2015b) and characters 152 and 153 in Giles et al. (2017) (dorsal aorta pierced by canal/s for exit of eff.a.2: present/absent; and dorsal aorta pierced by canal/s for exit of eff.a.1: present/absent) which require the precise identity of efferent arteries passing through foramina. This decision removes the uncertainty inherent to attempts to precisely identify arteries from osteological correlates in extinct taxa and increases the number of taxa for which the character can be coded. For example, the efferent epibranchial arteries are known to enter the anterior half of the neocranium of *Mimipiscis bartrami* and *M. toombsi*, but their identity cannot be inferred (Giles et al. 2017). Our new character is similar to character 17 of Caron et al. (2023) (ventral perforation of aortic canal anterior to exit level of X: present/absent); but unlike their statement this definition does not require the lateral entrance of the paired efferent artery to occur through foramina. To maximize applicability for incomplete specimens, it is not coded relative to the position of cranial nerve X as in Caron et al. (2023).

2. **Mode of efferent epibranchial artery entrance in anterior half of neocranium: groove/canal/foramen.** In some actinopterygians, such as *Coccocephalus wildi* and *Moythomasia durgaringa*, the entrance of efferent epibranchial arteries occurs in an open groove. In *Cosmoptychius striatus* and NSM 017.GF.017.004, this occurs in a canal. In *Luederia kempi*, foramina open ventrolaterally from the canals accommodating the lateral

dorsal aortae. In taxa where the previous character has been coded as absent, this should be coded as inapplicable.

3. **Aortic canal pierced ventrally by efferent arteries in posterior half of neocranium: absent/present.** A foramen in the ventral floor of the aortic canal does not occur in early diverging actinopterygians such as *Moythomasia durgaringa* and *Mimipiscis toombsi* (Gardiner 1984; Giles et al. 2022). As these taxa have grooves for efferent arteries in the anterior part of the neocranium, anterior to the bifurcation of the lateral dorsal aortae, this suggests that all efferent epibranchial arteries drained into the lateral dorsal aortae. In other taxa, such as *Coccocephalus wildi* (Poplin and Véran 1996) both an anterior groove and a posterior ventral entrance for efferent epibranchial arteries are argued to be present, supporting the independence of Characters 1 and 3. Together with Character 1, this is intended to replace characters 113 and 114 in Giles (2015b) and characters 152 and 153 in Giles et al. (2017) which require the precise identity of efferent arteries passing through foramina. Similar to our reasoning for our definition of Character 1, we feel that this replacement reduces uncertainty and increases applicability. It is similar to character 16 of Caron et al. (2023) (ventral perforation of aortic canal at or posterior to exit level of X: present/absent). To maximize applicability for incomplete specimens, it is not coded relative to the position of cranial nerve X as in Caron et al. (2023). Following Caron et al. (2023), we code an aortic notch as present for this character.

Characters retained from previous works:

4. **Ventral structure on neocranium indicating passage of dorsal aorta: absent/groove/canal.** This character refers to the presence of an aortic canal as in many Palaeozoic actinopterygians as well as the groove present in some Palaeozoic taxa (e.g.

709 *Cheirolepis trailli*. This is character 112 in Giles et al. (2015b), character 151 in Giles et
710 al. (2017) and character 14 in Caron et al. (2023). Also cited by Poplin (1974), Patterson
711 (1975), Gardiner (1984), Coates (1999), and Friedman (2007).

712 5. **Position of bifurcation of dorsal aorta into lateral dorsal aortae: anterior to end of**
713 **occiput/posterior to end of occiput.** This is character 115 in Giles et al. (2015b),
714 character 154 in Giles *et al.*, (2017), and character 13 in Caron et al. (2023). Also cited by
715 Coates (1999) and Friedman (2007).
716 6. **Enclosed bifurcation of dorsal aorta into lateral dorsal aortae: absent/present.** This
717 character is coded as present where the bifurcation of the lateral dorsal aortae is enclosed
718 by the aortic canal such that the grooves for the lateral dorsal aorta emerge from the canal
719 separately. This is character 116 in Giles et al. (2015b), character 155 in Giles et al.
720 (2017), and character 15 in Caron et al. (2023). Also cited by Patterson (1975) and Coates
721 (1999).
722 7. **Foramen or notch for orbital artery in the lateral commissure communicating with**
723 **the jugular canal: absent/present.** This is character 37 in Caron et al. (2023). Also cited
724 by Patterson (1975); Jarvik (1980), and Gardiner (1984).

725 **Conclusion**

726 Morphological variation in the dorsal arterial system of Palaeozoic actinopterygian provides a
727 rich source of characters. This allows for a comparative approach even when dealing with
728 fragmentary neocrania. This comparative approach is valuable at the locality of Blue Beach,
729 Nova Scotia, where neocrania are relatively common components of the actinopterygian fossil
730 record. NSM 017.GF.017.007 appears most similar to Devonian actinopterygians lacking ventral
731 foramina piercing the aortic canal, whereas NSM 017.GF.017.004 appears most similar to more

derived Carboniferous actinopterygians with lateral foramina for efferent epibranchial arteries and an enclosed bifurcation of the dorsal aorta into the lateral dorsal aortae. Consistent with observations in other major components of Carboniferous vertebrate faunas (Anderson et al. 2015; Clack et al. 2016; Challands et al. 2019; Smithson et al. 2024), these specimens imply a more gradual transition between Devonian and Carboniferous actinopterygian faunas (Wilson et al. 2018; Giles et al. 2022) than expected under a strict mass extinction and recovery scenario.

Acknowledgments

We thank the late Sonja Wood for her critical role in the Blue Beach Fossil Museum, for facilitating our research, and for her tireless efforts in improving her region and community. We thank Anthony Howell (RM), Tim Fedak (NSM), and Katherine Ogden (NSM) for specimen access and curatorial support. We thank Jason Pardo for helpful discussions. We also thank Dana Korneisel, Trystan Warnock-Juteau, and our peer reviewers for critical feedback on this manuscript.

Competing interests statement

The authors declare there are no competing interests.

Author contribution statement

CFM gathered and curated the fossil data. CDW and JSA acquired funding. CDW conceptualized the project, generated and analyzed the CT data, and wrote the original draft under the supervision of JSA. All authors reviewed and edited the final manuscript.

Funding statement

Research was supported by NSERC Discovery Grants 2017-04821 and 2023-04423 to Jason Anderson and an NSERC CGS M award to Conrad Wilson.

Data availability

Data generated or analyzed during this study, including 3D CT models, are provided in full within the published article and its supplementary materials. The original CT image stacks are available from the corresponding author upon request.

Literature Cited

Allis, E.P. 1897. The Cranial Muscles and Cranial and First Spinal Nerves in *Amia calva*. *Journal of Morphology* 12(3), pp. 489–737.

Allis, E.P. 1923. The Cranial Anatomy of *Chlamydoselachus anguineus*. *Acta Zoologica* 4(9), pp. 123-221

Anderson, J.S., Smithson, T., Mansky, C.F., Meyer, T. and Clack, J. 2015. A Diverse Tetrapod Fauna at the Base of "Romer's Gap." *PLOS One* 10(4), p. e0125446. doi: 10.1371/journal.pone.0125446.

Basden, A.M. and Young, G.C. 2001. A primitive actinopterygian neurocranium from the Early Devonian of southeastern Australia. *Journal of Vertebrate Paleontology* 21(4), pp. 754–766. doi: 10.1671/0272-4634(2001)021[0754:APANFT]2.0.CO;2.

Bjerring, H.C. 1971. The Nerve Supply to the Second Metamere Basicranial Muscle in Osteolepiform Vertebrates, with Some Remarks on the Basic Composition of the Endocranium. *Acta Zoologica* 52(2), pp. 189–225. doi: 10.1111/j.1463-6395.1971.tb00557.x.

Caron, A., Venkataraman, V., Tietjen, K. and Coates, M. 2023. A fish for Phoebe: a new

773 actinopterygian from the Upper Carboniferous Coal Measures of Saddleworth, Greater
774 Manchester, UK, and a revision of *Kansasiella eatoni*. *Zoological Journal of the Linnean Society*
775 198(4), pp. 957–981. doi: 10.1093/zoolinnean/zlad011.

776 Challands, T.J., Smithson, T.R., Clack, J.A., Bennett, C.E., Marshall, J.E.A., Wallace-Johnson,
777 S.M. and Hill, H. 2019. A lungfish survivor of the end-Devonian extinction and an Early
778 Carboniferous dipnoan radiation. *Journal of Systematic Palaeontology* 17(21), pp. 1825–1846.
779 Available at: https://www.tandfonline.com/doi/full/10.1080/14772019.2019.1572234.

780 Choo, B. 2012. Revision of the actinopterygian genus *Mimipiscis* (= *Mimia*) from the Upper
781 Devonian Gogo Formation of Western Australia and the interrelationships of the early
782 Actinopterygii. *Earth and Environmental Science Transactions of the Royal Society of*
783 *Edinburgh* 102(2), pp. 77–104. Available at:
784 https://www.cambridge.org/core/product/identifier/S1755691011011029/type/journal_article.

785 Choo, B., Lu, J., Giles, S., Trinajstic, K. and Long, J.A. 2019. A new actinopterygian from the
786 Late Devonian Gogo Formation, Western Australia. *Papers in Palaeontology* 5(2), pp. 343–363.
787 Available at: https://onlinelibrary.wiley.com/doi/abs/10.1002/spp2.1243.

788 Clack, J.A. et al. 2016. Phylogenetic and environmental context of a Tournaisian tetrapod fauna.
789 *Nature Ecology & Evolution* 1(1), p. 0002. Available at: http://www.nature.com/articles/s41559-
790 016-0002.

791 Coates, M.I. 1998. Actinopterygians from the Namurian of Bearsden, Scotland, with comments
792 on early actinopterygian neurocrania. *Zoological Journal of the Linnean Society* 122(1–2), pp.
793 27–59. Available at: http://linkinghub.elsevier.com/retrieve/pii/S0024408297901138.

794 Coates, M.I. 1999. Endocranial preservation of a Carboniferous actinopterygian from

795 Lancashire, UK, and the interrelationships of primitive actinopterygians. *Philosophical*
796 *Transactions of the Royal Society B: Biological Sciences* 354(1382), pp. 435–462. Available at:
797 http://rstb.royalsocietypublishing.org/cgi/doi/10.1098/rstb.1999.0396.

798 Coates, M.I. and Tietjen, K. 2018. "This strange little palaeoniscid": a new early actinopterygian
799 genus, and commentary on pectoral fin conditions and function. *Earth and Environmental*
800 *Science Transactions of the Royal Society of Edinburgh* 109(1–2), pp. 15–31. Available at:
801 https://www.cambridge.org/core/product/identifier/S1755691018000403/type/journal_article.

802 Danforth, C.H. 1912. The heart and arteries of *Polyodon*. *Journal of Morphology* 23(3), pp. 409–
803 454. doi: 10.1002/jmor.1050230303.

804 Eastman, C.R. 1907. Devonian Fishes of Iowa. *Iowa Geological Survey Annual Report* 28(1), pp.
805 29–386.

806 Friedman, M. 2007. *Styloichthys* as the oldest coelacanth: Implications for early osteichthyan
807 interrelationships. *Journal of Systematic Palaeontology* 5(3), pp. 289–343. doi:
808 10.1017/S1477201907002052.

809 Friedman, M. 2015. The early evolution of ray-finned fishes. *Palaeontology* 58(2), pp. 213–228.
810 doi: 10.1111/pala.12150.

811 Gardiner, B.G. 1966. Catalogue of Canadian fossil fishes. *Life Sciences Royal Ontario Museum*
812 *University of Toronto* 68, pp. 1–154.

813 Gardiner, B.G. 1984. The relationships of the palaeoniscid fishes, a review based on new
814 specimens of *Mimia* and *Moythomasia* from the Upper Devonian of Western Australia. *Bulletin*
815 *of the British Museum of Natural History, Geology* 37(November), pp. 173–428.

816 Giles, S., Coates, M.I., Garwood, R.J., Brazeau, M.D., Atwood, R., Johanson, Z. and Friedman,
817 M. 2015a. Endoskeletal structure in *Cheirolepis* (Osteichthyes, Actinopterygii), An early ray-
818 finned fish. *Palaeontology* 58(5), pp. 849–870. Available at:
819 http://doi.wiley.com/10.1111/pala.12182.

820 Giles, S., Darras, L., Clément, G., Blieck, A. and Friedman, M. 2015b. An exceptionally
821 preserved Late Devonian actinopterygian provides a new model for primitive cranial anatomy in
822 ray-finned fishes. *Proceedings of the Royal Society B: Biological Sciences* 282(1816), p.
823 20151485. Available at:
824 http://rspb.royalsocietypublishing.org/lookup/doi/10.1098/rspb.2015.1485.

825 Giles, S., Feilich, K., Warnock, R.C.M., Pierce, S.E. and Friedman, M. 2022. A Late Devonian
826 actinopterygian suggests high lineage survivorship across the end-Devonian mass extinction.
827 *Nature Ecology & Evolution* 7(1), pp. 10–19. Available at:
828 https://doi.org/10.1101/2021.09.02.458676.

829 Giles, S., Friedman, M. and Brazeau, M.D. 2015c. Osteichthyan-like cranial conditions in an
830 Early Devonian stem gnathostome. *Nature* 520(7545), pp. 82–25. doi: 10.1038/nature14065.

831 Giles, S., Xu, G.-H., Near, T.J. and Friedman, M. 2017. Early members of 'living fossil' lineage
832 imply later origin of modern ray-finned fishes. *Nature* 549(7671), pp. 265–268. Available at:
833 http://www.nature.com/doifinder/10.1038/nature23654.

834 Grande, L. 2010. An Emperical Synthetic Pattern Study of Gars (Lepisosteiformes) and Closely
835 Related Species, Based Mostly on Skeletal Anatomy. The Resurrection of Holostei. *Copeia*
836 10(2A). doi: 10.7572/2167-5880-127.3.219.

837 Hamel, M.-H. and Poplin, C. 2008. the Braincase Anatomy of *Lawrenciella schaefferi*,

838 actinopterygian from the Upper Carboniferous of Kansas (USA). *Journal of Vertebrate*
839 *Paleontology* 28, pp. 989–1006. doi: 10.1671/0272-4634-28.4.989.

840 Henderson, S., Dunne, E.M., Fasey, S.A. and Giles, S. 2022a. The early diversification of ray-
841 finned fishes (Actinopterygii): hypotheses, challenges and future prospects. *Biological Reviews*
842 8. doi: 10.1111/brv.12907.

843 Henderson, S., Dunne, E.M. and Giles, S. 2022b. Sampling biases obscure the early
844 diversification of the largest living vertebrate group. *Proceedings of the Royal Society B:*
845 *Biological Sciences* 289(1985), p. 20220916. doi: 10.1098/rspb.2022.0916.

846 Jarvik, E. 1980. *Basic Structure and Evolution of Vertebrates, Volume 1*. London: Academic
847 Press.

848 Liem, K.F., Bemis, W.E., Walker, Jr., W.F. and Grande, L. 2001. The Circulatory System of
849 Early Fishes. In: *Functional Anatomy of the Vertebrates*. 3rd Edition. Belmont, California:
850 Brooks/Cole Cengage Learning, pp. 608–611.

851 Long, J.A. 1988. New palaeoniscoid fishes from the Late Devonian and Early Carboniferous of
852 Victoria. *Memoirs of the Association of Australasian Palaeontologists* 7, pp. 1–64.

853 Long, J.A. and Trinajstic, K. 2010. The Late Devonian Gogo Formation Lägerstatte of Western
854 Australia: Exceptional Early Vertebrate Preservation and Diversity. *Annual Review of Earth and*
855 *Planetary Sciences* 38(1), pp. 255–279. Available at:
856 http://www.annualreviews.org/doi/10.1146/annurev-earth-040809-152416.

857 Mansky, C.F. and Lucas, S.G. 2013. Romer's Gap revisited: continental assemblages and ichno-
858 assemblages from the basal Carboniferous of Blue Beach, Nova Scotia, Canada. In: Lucas, S. G.,

DiMichele, W. A., Barrick, J. E., Schneider, J. W., and Spielmann, J. A. eds. *Bulletin 60: The Carboniferous-Permian Transition*. Albuquerque: New Mexico Museum of Natural History and Science, pp. 244–273.

Martel, A.T. and Gibling, M.R. 1991. Wave-dominated lacustrine facies and tectonically controlled cyclicity in the Lower Carboniferous Horton Bluff Formation, Nova Scotia, Canada. *Special Publications of the International Association of Sedimentologists* 13, pp. 223–243.

Martel, A.T. and Gibling, M.R. 1996. Stratigraphy and tectonic history of the Upper Devonian to Lower Carboniferous Horton Bluff Formation, Nova Scotia. *Atlantic Geology* 32(1), pp. 13–38.

Mickle, K.E. 2017. The lower actinopterygian fauna from the Lower Carboniferous Albert shale formation of New Brunswick, Canada -- a review of previously described taxa and a description of a new genus and species. *Fossil Record* 20(1), pp. 47–67. Available at: http://www.foss-rec.net/20/47/2017/.

Mistiaen, B., Brice, D., Zapalski, M.K. and Loones, C. 2012. Brachiopods and Their Auloporoid Epibionts in the Devonian of Boulonnais (France), Comparison with Other Associations Globally. In: Talent, J. A. ed. *Earth and Life: Global Biodiversity, Extinction Intervals and Biogeographic Perturbations Through Time*. Heidelberg: Springer Netherlands, pp. 159–188.

Nielsen, E. 1942. *Studies on Triassic Fishes from East Greenland I. Glaucolepis and Boreosomus*. Copenhagen, DK: C.A. Reitzels.

Nielsen, E. 1949. *Studies on Triassic Fishes from East Greenland II. Australosomus and Birgeria*. Copenhagen, DK: C.A. Reitzels Forlag.

Patterson, C. 1975. The braincase of pholidophorid and leptolepid fishes, with a review of the

880 actinopterygian braincase. *Philosophical Transactions of the Royal Society of London B:*
881 *Biological Sciences* 269(899), pp. 275–579. doi: 10.1038/192023a0.

882 Poplin, C. 1975. Remarques sur le système artériel épibranchial chez les actinoptérygiens
883 primitifs fossiles. *Colloque international C.N.R.S.* 218, pp. 265–271. doi:
884 10.1371/journal.pone.0142897.

885 Poplin, C.M. 1974. *Étude de Quelques Paléoniscidés Pennsylvaniens du Kansas*. Paris: Éditions
886 du Centre National de la Recherche Scientifique.

887 Poplin, C.M. 1984. *Lawrenciella schaefferi* n.g., n.sp. (Pisces: Actinopterygii) and the use of
888 endocranial characters in the classification of the Palaeonisciformes. *Journal of Vertebrate*
889 *Paleontology* 4(3), pp. 413–421. Available at:
890 http://www.tandfonline.com/doi/abs/10.1080/02724634.1984.10012019.

891 Poplin, C.M. and Véran, M. 1996. A revision of the actinopterygian fish *Coccocephalus wildi*
892 from the Upper Carboniferous of Lancashire. *Special Papers in Palaeontology* 52, pp. 7–29.

893 Pradel, A., Maisey, J.G., Mapes, R.H. and Kruta, I. 2016. First evidence of an intercalar bone in
894 the braincase of "palaeonisciform" actinopterygians, with a virtual reconstruction of a new
895 braincase of *Lawrenciella* Poplin, 1984 from the Carboniferous of Oklahoma. *Geodiversitas*
896 38(4), pp. 489–504. Available at: http://www.bioone.org/doi/10.5252/g2016n4a2.

897 Rayner, D.H. 1951. On the Cranial Structure of an Early Palaeoniscid, *Kentuckia*, gen. nov.
898 *Transactions of the Royal Society of Edinburgh* 62(01), pp. 53–83. Available at:
899 http://www.journals.cambridge.org/abstract_S0080456800009248.

900 Ridewood, W.G. 1899. On the Relations of the Efferent Branchial Blood-vessels to the "Circulus

Cephalicus" in Teleostan Fishes. *Proceedings of the Zoological Society of London*, pp. 939–956. doi: 10.1038/154714a0.

Sallan, L.C. and Coates, M.I. 2010. End-Devonian extinction and a bottleneck in the early evolution of modern jawed vertebrates. *Proceedings of the National Academy of Sciences* 107(22), pp. 10131–10135. Available at: http://www.pnas.org/cgi/doi/10.1073/pnas.0914000107.

Sallan, L.C. and Coates, M.I. 2013. Styracopterid (Actinopterygii) ontogeny and the multiple origins of post-Hangenberg deep-bodied fishes. *Zoological Journal of the Linnean Society* 169(1), pp. 156–199. Available at: https://academic.oup.com/zoolinnean/article-lookup/doi/10.1111/zoj.12054.

Schaeffer, B. 1971. The Braincase of the Holostean Fish *Macrepistius*, with Comments on Neurocranial Ossification in the Actinopterygii. *American Muesum Novitates* 2459(2459), pp. 1–34.

Schaeffer, B. and Dalquest, W.W. 1978. A palaeonisciform braincase from the Permian of Texas, with comments on cranial fissures and the posterior myodome. *American Museum Novitates* 2658, pp. 1–15.

Schneider, C.A., Rasband, W.S. and Eliceiri, K.W. 2012. NIH Image to ImageJ: 25 years of image analysis. *Nature Methods* 9(7), pp. 671–675. doi: 10.1038/nmeth.2089.

Schultze, H.-P., Mickle, K.E., Poplin, C.M., Hilton, E.J. and Grande, L. 2022. *Handbook of Paleoichthyology Volume 8A: Actinopterygii I, Palaeoniscimorpha, Stem Neopterygii, Chondrostei*. Schultze, H.-P. ed. München, Germany: Verlag Dr. Friedrich Pfeil.

Smithson, T.R., Ruta, M. and Clack, J.A. 2024. On *Ossirarus kierani*, a stem tetrapod from the

922 Tournaisian of Burnmouth, Berwickshire, Scotland, and the phylogeny of early tetrapods. *Fossil*
923 *Record* 27(3), pp. 333–352. Available at: https://fr.pensoft.net/article/126410/.

924 Tang, W., Pe-Piper, G., Piper, D.J.W., Chen, A., Hou, M., Guo, Z. and Zhang, Y. 2024.
925 Architecture of lacustrine deposits in response to early Carboniferous rifting and Gondwanan
926 glaciation, Nova Scotia, south-east Canada. *Sedimentology* 71(2), pp. 457–485. doi:
927 10.1111/sed.13140.

928 Thiruppathy, M., Fabian, P., Andrew Gillis, J. and Gage Crump, J. 2022. Gill developmental
929 program in the teleost mandibular arch. *eLife* 11, pp. 1–9. doi: 10.7554/eLife.78170.

930 Watson, D.M.S. 1925. The Structure of Certain Palaeoniscoids and the Relationships of that
931 Group with other Bony Fish. *Proceedings of the Zoological Society of London* 54, pp. 815–870.

932 Watson, D.M.S. 1928. On some Points in the Structure of Palaeoniscid and allied Fish.
933 *Proceedings of the Zoological Society of London* 98(1), pp. 49–70.

934 Wilson, C.D., Mansky, C.F. and Anderson, J.S. 2021. A platysomid occurrence from the
935 Tournaisian of Nova Scotia. *Scientific Reports* 11(1), p. 8375. Available at:
936 https://doi.org/10.1038/s41598-021-87027-y.

937 Wilson, C.D., Pardo, J.D. and Anderson, J.S. 2018. A primitive actinopterygian braincase from
938 the Tournaisian of Nova Scotia. *Royal Society Open Science* 5(5), p. 171727. Available at:
939 https://royalsocietypublishing.org/doi/10.1098/rsos.171727.

940 **Supplementary files**

941 Supplementary File 1: Virtual model of NSM 017.GF.017.007 in .ply format

942 Supplementary File 2: Virtual model of NSM 017.GF.017.004 in .ply format

943 **Figures**

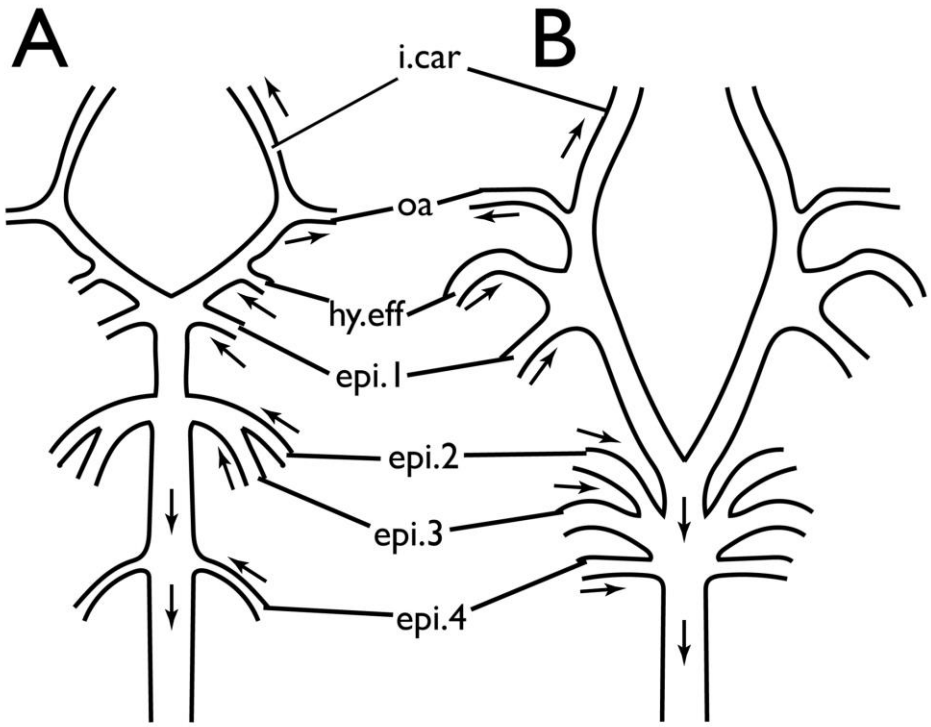

944

945 Fig. 1. Schematic illustration of early actinopterygian dorsal arterial system following Poplin
946 (1975) for A. *Kansasiella eatoni* and B. *Pteronisculus stensioi*. Arrows indicate inferred
947 direction of blood flow. epi.1-epi.4, efferent epibranchial arteries I-IV; hy.eff, efferent hyoidean
948 artery; i.car, internal carotid; oa, orbital artery.

949

950

951

952

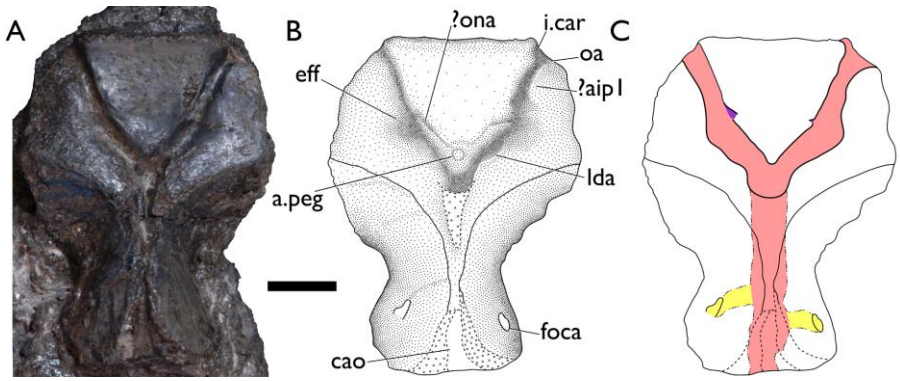

953

954 Fig. 2. NSM 017.GF.017.007. Scale bar = 5 mm. A. Photograph of specimen in ventral view. B.
955 Interpretive drawing of specimen in ventral view. C. Trace of specimen, including vascular
956 canals, from μCT data in ventral view. a.peg, peg for aortic ligament; ?aip1, articulation facet for
957 the first infrapharyngobranchial; cao, aortic canal; eff, groove for efferent epibranchial arteries;
958 foca, foramen for occipital artery; i.car, groove for internal carotid; lda, lateral dorsal aortae; oa,
959 groove for orbital artery; ?ona, groove for orbitonasal artery. In C, red indicates the dorsal aorta,
960 yellow the occipital artery, and purple the orbitonasal arteries.

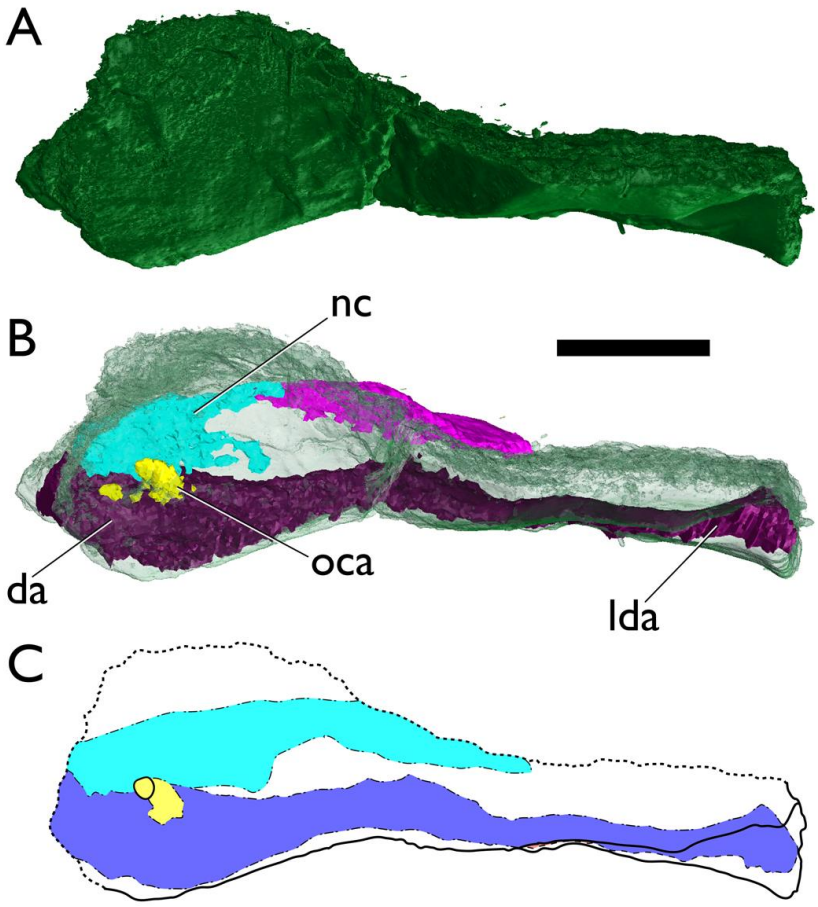

Fig. 3. NSM 017.GF.017.007. Scale bar = 5 mm. A. µCT rendering of specimen in right lateral view. B. µCT transparency rendering of specimen and blood vessels in right lateral view. C. Trace of specimen, including blood vessels, from µCT data in right lateral view. da, dorsal aorta; lda, lateral dorsal aortae; nc, notochord canal; oca, occipital artery. In C, dark blue indicates the dorsal aorta, yellow the occipital artery, and turquoise the notochordal space.

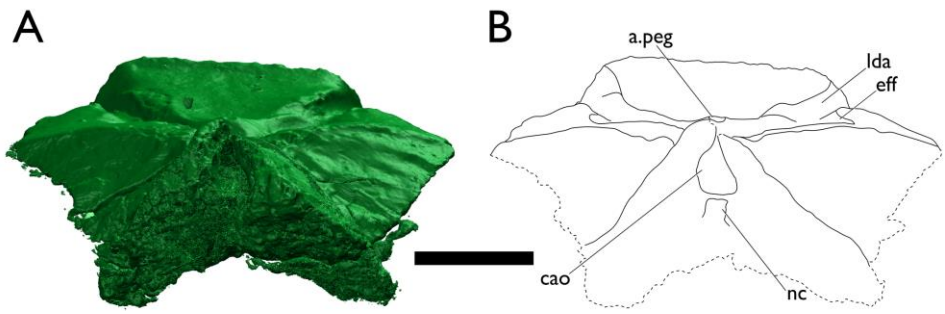

969

970 Fig. 4. NSM 017.GF.017.007. Scale bar = 5 mm. A. µCT rendering of specimen in posterior
971 view, ventral rotated towards top. B. Interpretive line drawing of specimen in posterior view,
972 ventral rotated towards top. a.peg, peg for aortic ligament; cao, aortic canal; eff, groove for
973 efferent epibranchial arteries; lda, lateral dorsal aortae; nc, notochord canal.

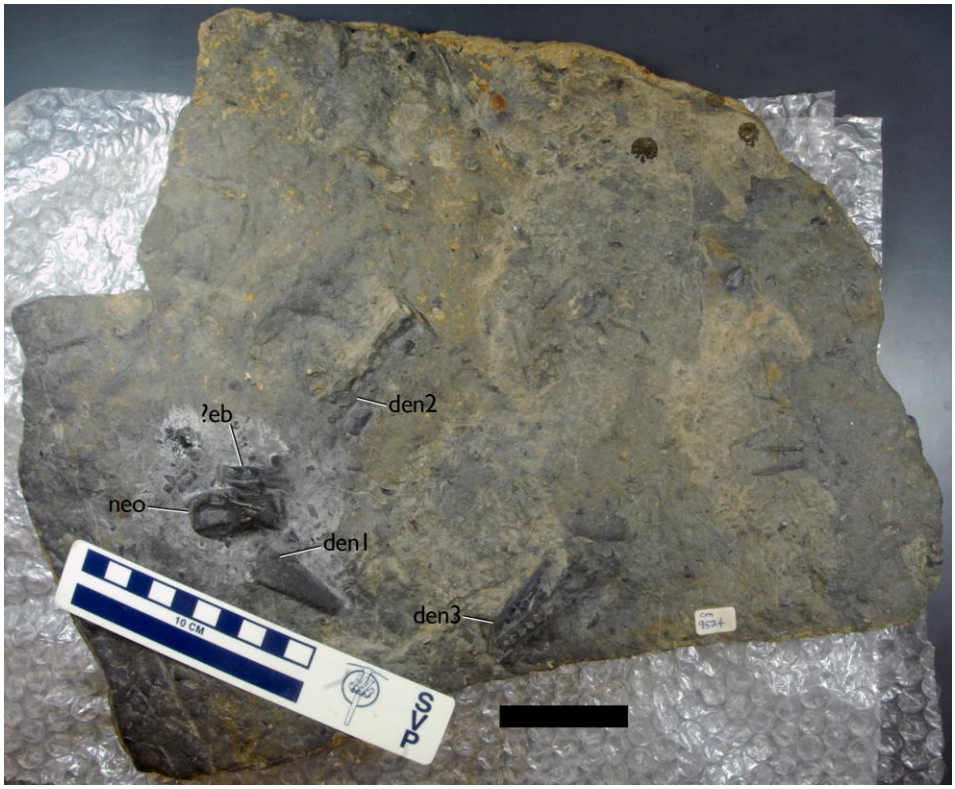

Fig. 5. Photograph of the large gully-slide bonebed block containing NSM 017.GF.017.004. Scale bar = 5 cm. den1-3, dentary 1-3; ?eb, epibranchial ossification; neo, neocranium.

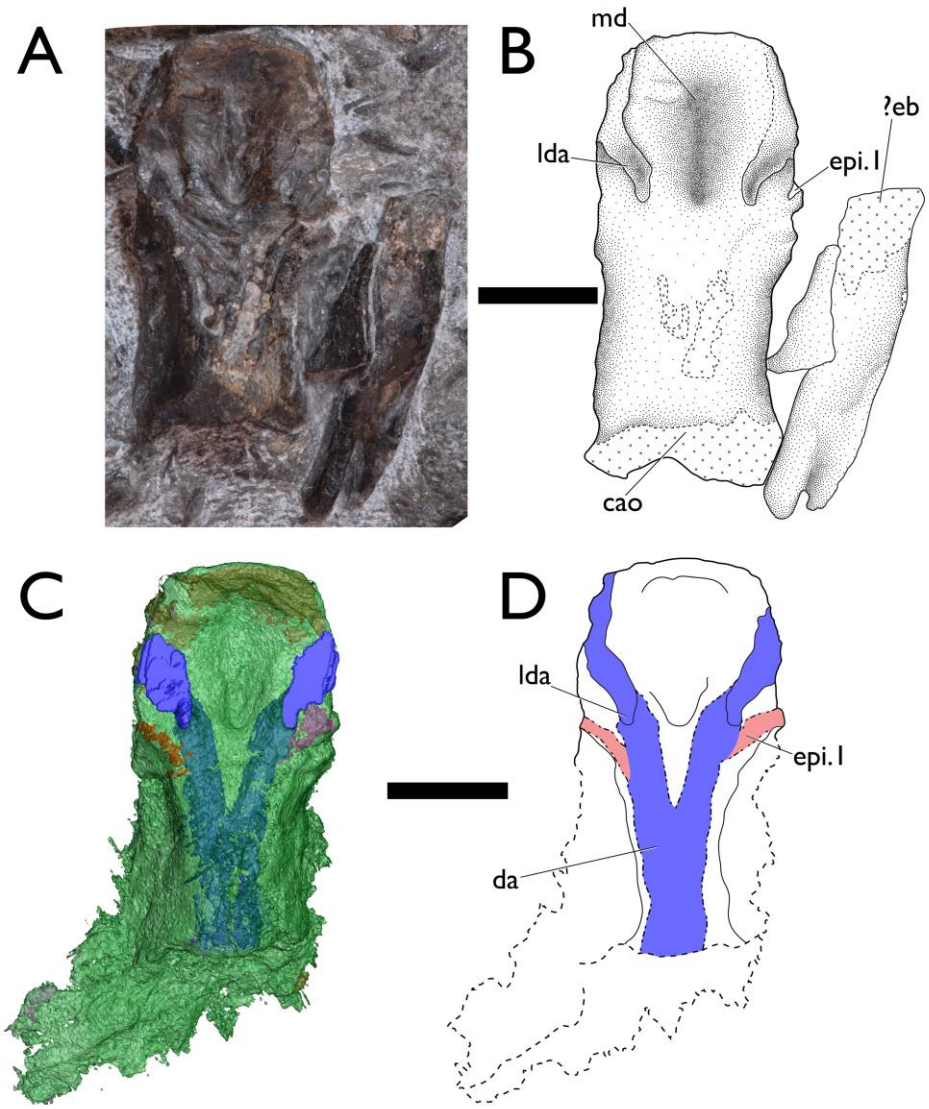

983

984 Fig. 6. NSM 017.GF.017.004. Scale bar = 5 mm. A. Photograph of neocranium in ventral view.
985 B. Interpretive drawing of neocranium in ventral view. C. µCT transparency rendering of
986 specimen and blood vessels in ventral view. D. Trace of specimen, including blood vessels, from

µCT data in ventral view. cao, aortic canal; da, dorsal aorta; epi.1, efferent epibranchial artery I; ?eb, epibranchial ossification; lda, lateral dorsal aortae; md, median depression. In D, dark blue indicates the dorsal aorta and red the efferent epibranchial artery.

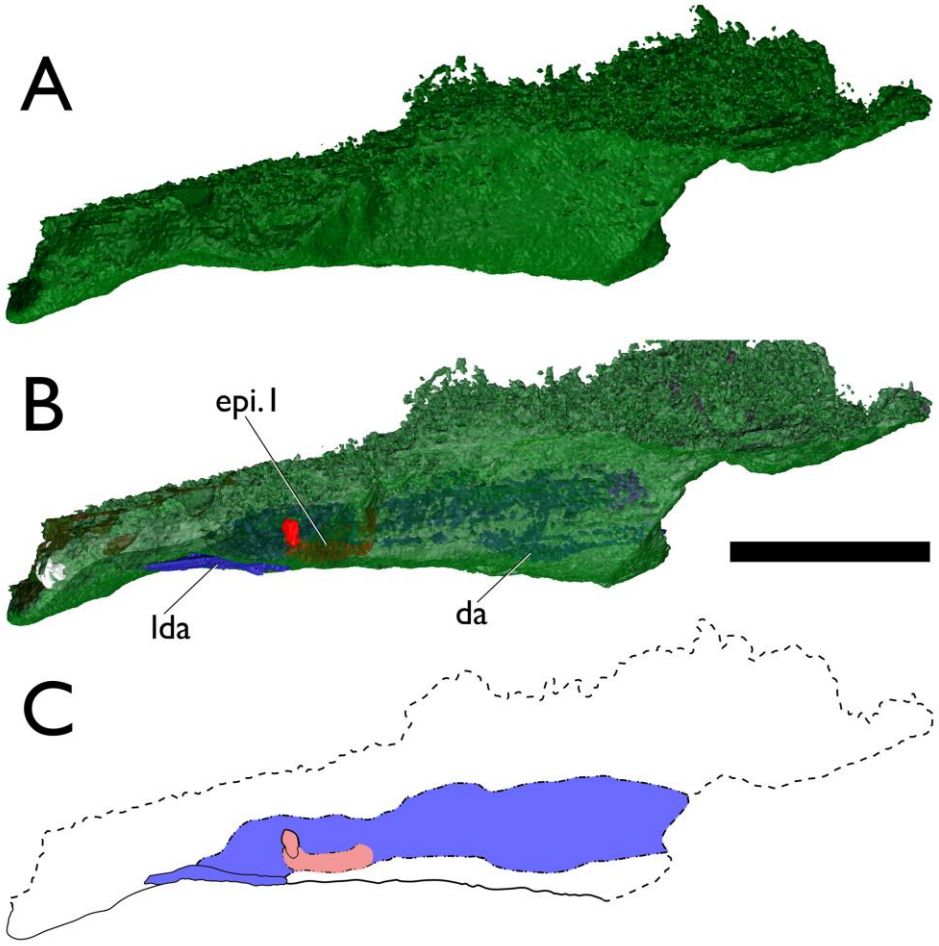

Fig. 7. NSM 017.GF.017.004. Scale bar = 10 mm. A. µCT rendering of specimen in left lateral view. B. µCT transparency rendering of specimen and blood vessels in left lateral view. C. Trace

of specimen, including blood vessels, from µCT data in left lateral view. da, dorsal aorta; epi.1, efferent epibranchial artery I. lda, lateral dorsal aortae. In C, dark blue indicates the dorsal aorta and red the efferent epibranchial artery.

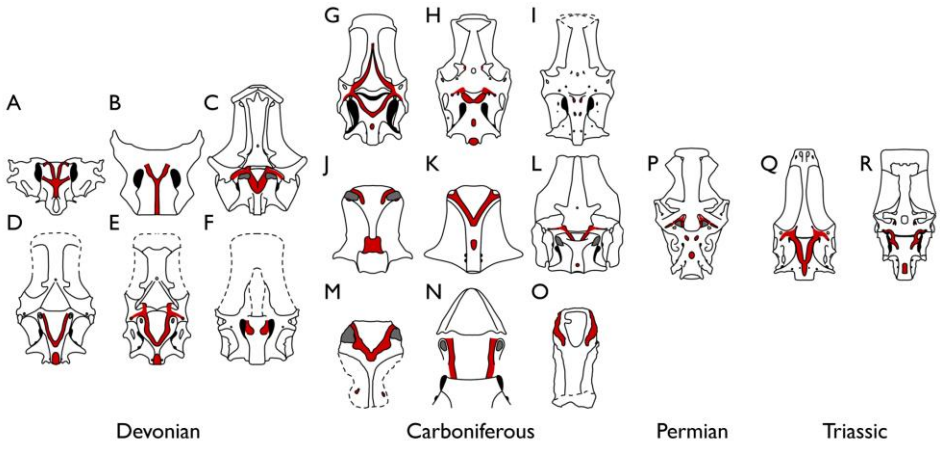

Fig. 8. Selected non-neopterygian braincases in ventral view. D, E, G, K, M modified and from Wilson et al. (2018); remaining specimen illustrations are based on published illustrations cited in caption. Solid lines indicate illustrated anatomy and correlates of arterial circulation. Red fill indicates arterial circulation, grey fill indicates articulation facet of first infrapharyngobranchial, black fill indicates ventral otic fissure, otico-occipital fissure, and vestibular fontanelles. Dashed lines in braincase illustrations and absent lines in blood vessel illustrations indicate uncertainty. A. Neocranium of *Cheirolepis trailli* (Giles et al. 2015a). B. Neocranium of *Howqualepis rostridens* (Long 1988; Giles et al. 2015a). C. Braincase and parasphenoid of *Mimipiscis toombsi* (Gardiner 1984; Choo 2012). D. Braincase and parasphenoid of *Raynerius splendens* (Giles et al. 2015b). E. Braincase and parasphenoid of *Moythomasia durgaringa* (Gardiner 1984; Long and Trinajstic 2010). F. Partial braincase of *Pickeringius acanthophorus* (Choo et al. 2019). G.

1010 Braincase of *Coccocephalus wildi* with parasphenoid removed (Poplin and Véran 1996). H.
1011 Braincase of *Lawrenciella schaefferi* with parasphenoid removed. I. Braincase of *Kansasiella*
1012 *eatoni* with parasphenoid removed (Poplin 1974). J. Partial braincase of *Cosmoptychius striatus*
1013 (presumably juvenile) (Watson 1928; Schaeffer 1971). . K. Partial braincase of *Kentuckia deani*
1014 (Rayner 1951). L. Braincase and parasphenoid of *Woodichthys bearsdeni* (Coates 1998). M.
1015 Partial neocranium and parasphenoid of *Avonichthys manskyi* (Wilson et al. 2018). N. NSM
1016 017.GF.017.004. O. NSM 017.GF.017.007. P. Braincase of *Luederia kempi* with parasphenoid
1017 removed (Schaeffer and Dalquest 1978). Q. Braincase of *Australosomus kochi* with parasphenoid
1018 removed (Nielsen 1949). R. Braincase of *Pteronisculus stensioi* with parasphenoid removed
1019 (Nielsen 1942).

Formatted: Font: (Default) +Headings CS (Times New Roman), 12 pt